International Journal of Hydrogen Energy 117 (2025) 430–441

Contents lists available at ScienceDirect

International Journal of Hydrogen Energy

journal homepage: www.elsevier.com/locate/he

Al6060 cut wire granules for Al-water reaction: Evaluation of reaction conditions and granule treatments

M. Agote-Arán [a,*], B. Welte [a], R. Freeman [a], N. Mutti [a], M. Haller [b], A. Heel [a]

[a] UMTEC Institute for Environmental and Process Engineering, Eastern Switzerland University of Applied Sciences (OST), Rapperswi, 8640, Switzerland
[b] SPF Institute for Solar Technology, Eastern Switzerland University of Applied Sciences (OST), Rapperswil, 8640, Switzerland

ARTICLE INFO

Handling Editor: Dr A Iranzo

Keywords:
Seasonal energy storage
Renewable metal fuels
Al-water reaction
Al alloys

ABSTRACT

Aluminium (Al) is a promising Renewable Metal Fuel (ReMeF) for seasonal energy storage due to its high abundance and energy density. Most Al-water reaction studies use Al powder for fast kinetics, but its ignition risks pose safety challenges. This article explores using commercially available cut wire Al6060 granules above the explosion size threshold as a cheap, safe and reactive source of Al fuel. Most suitable conditions were defined for reaction in alkaline aqueous media. Importantly, activity data combined with microscopy studies reveal a reaction mechanism characterized by pore formation and fast reaction kinetics. We propose that Al6060 cut wire microstructure directs the corrosive attack towards pore formation making these granules safe and yet highly active under reaction conditions. This work brings new insight into how Al manufacturing could be adjusted to promote faster oxidation rates and produce Al granules suitable for ReMeF applications.

1. Introduction

In order to minimize the impact of global warming, fossil fuels need to be replaced by renewable energy sources such as hydropower, wind and solar energies. However, the production of renewable energy is highly seasonal and, in many countries, it does not align with highest energy demand periods. Thus, it requires the development of efficient systems to store energy over longer times spans of months and that can be transported over long distances. A promising option is the use of aluminium (Al) as a renewable and recyclable metal fuel (ReMeF) [1,2]. Al is a non-hazardous and abundant element which can be oxidized by water to produce hydrogen (H_2) and heat [3,4]. The H_2 produced can then be converted into electricity and heat by fuel cells. The volumetric energy density of Al doubles the density of other energy carriers such as hydrocarbons, or mineral oils, making it particularly suitable for seasonal energy storage [5]. As proposed by Haller et al. the material cycle can be closed in an environmental manner by reducing aluminium oxides or hydroxides obtained during the H_2 production back to Al [5–9] via a carbon free electrolysis process [10,11].

The reaction of Al in aqueous media (<100 °C) leads to the formation $Al(OH)_3$ as a byproduct besides H_2 [12](eq. (1)).

$$2Al + 6H_2O(l) \rightarrow 2Al(OH)_3 + 3H_2 \quad \text{eq. 1}$$

This process is highly exothermic ($\Delta H_r \sim 280$ kJ/mol of H_2 at ~50–100 °C [13,14]), and although it is thermodynamically favourable, the formation of a surface aluminium oxide layer inhibits the reaction as it prevents water from coming into direct contact with the metallic Al [12,15–17]. Many researchers have proposed methods for a continuous removal of the oxide layer to attain effective and fast H_2 production. These methods include the use of hydroxide promoters, acid promoters, salt/oxide promoters, liquid metals or ultrasonics [15–29]. Activation of Al precursor by mechanical treatments has also been exploited, e.g. by ball milling techniques [16,22,30–35]. Faster reaction kinetics can also be achieved by alloying aluminium with different elements. The elements most studied comprise Ga, In, Sn, Cu, Bi, Mg, Li and Si [23,26,36–44] which are incorporated into the Al by ball milling or high temperature melting procedures. These elements permeate through Al grain boundaries, inhibiting passivation of the aluminium grain surfaces. The use of carbon additives such as carbon nanotubes, carbon nanoparticles, graphene, and graphite is also efficient to improve hydrogen generation performance of Al [45–51].

The Al microstructure and the accumulation of different metastable precipitate phases in Al grain boundaries is known to make the Al susceptible to intergranular and pitting corrosion, which can be beneficial for fast Al-water reaction. For Mg and Si containing Al alloys for example, the formation of Mg_2Si or Mg_2Al phases in the grain

* Corresponding author.
E-mail address: miren.agote@ost.ch (M. Agote-Arán).

https://doi.org/10.1016/j.ijhydene.2025.03.117
Received 7 November 2024; Received in revised form 4 March 2025; Accepted 7 March 2025
Available online 19 March 2025
0360-3199/© 2025 The Authors. Published by Elsevier Ltd on behalf of Hydrogen Energy Publications LLC. This is an open access article under the CC BY license (http://creativecommons.org/licenses/by/4.0/).

boundaries sensitizes the material to corrosion [52–55]. In a study by Meroueh et al. Mg-doped and Mg_2Si-doped Al were prepared by cold-rolling and annealing procedure to control grain size; reducing grains to 30 μm was observed to increase the H_2 production rate by an order of magnitude [56].

In addition to the above, the reaction rates can be controlled by adjusting the particle size of the Al used as the fuel. Since Al-water reaction occurs on the surface of the solid, the use of small particles with high effective surface area guarantees fast kinetics. In fact, most of the studies available on Al-water reactions focus on the use of Al powder [12,57–63]. The downside of using metal powders is that their production is energy intensive and costly. More importantly, metal powders with particle size <0.2 mm can create explosive mixtures with air [3], which requires the implementation of extensive safety measures (i.e. transport and storage) for the use of Al as a ReMeF. Development of hierarchical bulk nanoporous Al fuel has been explored by Corsi et al. [64]. Although the high surface area makes these materials highly reactive, its rapid oxidation also comprises explosion concerns. While the use of $LiBH_4$ can prevent pyrophoric ignition [65], this path requires further developments for its future implementation.

Most studies on Al-water reactions focus on the use as of Al powders (<200 μm) which comprise risk of explosion, as well as on the use of expensive activation approaches. An illustration of this is given by the recent comprehensive review by Kaur et al. [12], a summary table based on this review (including Al size and activation methods) is given in the supplementary information (Table S1).

The use of larger granules based on commercially available Al sources comprises a more viable solution for the implementation of this reaction in the energy sector. Besides, it allows for coupling renewable energy storage in metals with water-to-energy concepts. In this regards, recent studies by Urbonavicius et al. and Mezulis et al., report Al-water rection kinetics using Al waste as the cheap source of Al fuel [66,67]. Their studies evaluate the reactivity of Al scrap from household application under several reaction parameters. Our own combined experimental and life cycle analysis for Al-water reactions based on Al from recycling streams bring deeper insight on the applicability and challenges of using Al waste as fuel [8].

Care needs to be taken when assessing commercial Al sources since Al alloys are complex materials, engineered with specific properties for particular applications. Consequently, the Al-water reactivity of commercial sources can vary significantly, influenced not only by their alloy composition but also by the structural properties resulting from the manufacturing process [68–71].

To our knowledge, there are no systematic studies on the impact of commercial Al structures on the Al-water reaction kinetics. Hence, this research is based on the use of commercial Al alloy as an economical source of metal fuel. Granules >0.5 mm were selected because they exceed the size threshold for explosion risk, making them safe for storage and transport; the Al6060 composition was chosen due the commercial availability of this alloy and its high Mg and Si content. The research presented here evaluates the reaction conditions suitable for these granules and aims to understand the effects of Al6060 structural variations on the reaction kinetics.

The tests were performed in sodium hydroxide (NaOH) solutions [7,8]. The reaction of Al with NaOH solutions to produce hydrogen leads to sodium aluminate products in solution (eq. (2)) [72].

$$2Al + 2NaOH + 6H_2O \rightarrow 2NaAl(OH)_4 + 3H_2 \quad \text{eq. 2}$$

$$NaAl(OH)_4 \rightarrow NaOH + Al(OH)_3 \quad \text{eq. 3}$$

The NaOH consumed is regenerated when aluminium hydroxide ($Al(OH)_3$) precipitates (eq. (3)). Therefore, the overall process is eq. (1) and only aluminium and water are the consumed raw materials to produce H_2 and $Al(OH)_3$.

The Al-water reaction rates in aqueous alkaline solutions are known to depend on reaction temperature and the degree of alkalinity [17]. In case of the temperature, the reaction rate increases exponentially with the temperature as expressed by the Arrhenius equation. As for the alkalinity, several publications report faster kinetics with increasing alkalinity [72,73] which is attributed to a more efficient oxide layer removal at higher pH.

In this study, Al-water reactions were conducted in NaOH solutions under varying temperature and alkaline conditions. Crucially, the morphological and structural factors contributing to the high reactivity of this specific Al alloy were thoroughly examined by subjecting the granules to different mechanical and thermal treatments.

2. Materials and methods

2.1. Materials

Temperature and alkalinity studies were performed using same batch of Al6060 grade cut wire granules (⌀ ca. 1.0 mm) purchased from KrampeHarex (Germany)/Carlo Bernasconi AG (Switzerland). They consist of cylindrical granules obtained by cutting of extruded wires. A portion of these granules was subjected to an annealing procedure. The annealing was performed by heating at 530 °C in an oven for 20 min under Ar. After the treatment, the samples were quenched by dropping them from the oven directly into a cold-water bath.

For granule morphology and mechanical treatment studies, two types of Al6060 granules were purchased from Kuhmichel (Germany). One of the morphologies consisted of the cylindrical cut wire, and the other comprised spherical granules obtained by mechanical treatment of cylindrical cut wires to reshape them into spherical granules. For each morphology, 0.6, 0.8, 1.0 and 1.2 mm diameter granules were investigated. Making reference to their shape, in this manuscript the cut wire samples are referred to as cylindrical (cut wires with no further treatment) or rounded (mechanically treated).

The Al6060 alloy composition - specified by the suppliers - comprised 97.9–99.3% Al, 0.35–0.6% Mg, 0.3–0.6% Si, 0.1–0.3% Fe, 0.15% Zn, and <0.1% Cr, Cu, Mn and Ti.

2.2. Al-water reaction setup

The Al-water reaction rate tests were performed in a closed setup comprising a three–neck round-bottomed flask fitted with a magnetic stirrer. The temperature in the flask was controlled by a heated water bath with a thermocouple for bath temperature control. The reading of this thermocouple was taken as reaction temperature. Loss of solution due to evaporation was minimized by the use of a dimroth condenser. ANKOM^{RF} Gas Production System pressure sensor was mounted on top of the condenser via a custom-made glass adapter. All connections were sealed with silicon sealing paste to prevent gas leakages during experiments. Schematics of the setup are given in the supplementary information (Fig. S1).

For the tests, 50 mL NaOH solution (Sigma-Aldrich, >97%) prepared using distilled water were preheated to the desired temperature. Then, Al was dosed through one of the side necks and the system was closed immediately. The mixture was kept under vigorous stirring during reaction to ensure homogeneous temperature and product concentration in the flask. Pressure increase due to the H_2 produced as well as gas temperature were recorded by the ANKOM^{RF} every 15 s. The reading was used to quantify the evolution of H_2 production by the ideal gas equation. Where P is the pressure (atm), T is the temperature (K), R is the universal gas constant (0.0821 atm L $mol^{-1}{\cdot}K^{-1}$) and V is the volume of the reactor excluding the added solution (0.658 L).

Note that for safety reasons, the ANKOM^{RF} sensor periodically vents small amounts of H_2 to avoid overpressure in the glass ware. Hence, a safety valve opens for 500 ms when 500 mbars are reached in the system. The venting occurs up to four times per experiment which leads to steps in the H_2 evolution curves obtained, and a 17% deviation from the expected total H_2 production. In order to account for the H_2 loss during

the valve openings, the production rate of H_2 at the timestep of valve openings were interpolated using EXCEL TREND function; such function extends a linear trend line using the method of least squares to calculate the additional y-values for a new set of x-values. In this case the TREND function was implemented using five datapoints prior each valve opening event to extrapolate two data points during the valve opening. The obtained hydrogen production was then added to the total hydrogen production of the logged data after valve closure. Fig. S2 in the supporting information illustrates the steps in the measured data as well as the data after correction by trend function. All the data presented in the main manuscript corresponds to corrected data. The original vs corrected data for all tests is given in Fig. S3. Finally, in order to ensure system reproducibility, the tests performed with different granule morphologies (Kuhmichel granules) were performed three times. The data shown in this paper represents the average of the three tests. Note that the data obtained in each repeat was corrected according to the procedure shown in Fig. S2 prior averaging. The standard deviations obtained ranged between 0.00020 mol and 0.00061 mol and the deviation between the observed and theoretical total amount of H_2 was between 4 and 11%. An Al6060 composition comprising 98 wt% of Al was assumed for calculating the later deviation. The individual tests are shown in the supporting information (Fig. S4) together with the deviation values (Table S2).

2.3. Material characterisation

Microscopy: images were taken to evaluate morphological analysis of Al granules at different times of reaction. The general morphology was observed in a Leica DVM 6 M digital microscope. Selected samples were evaluated in a JSM IT200 Scanning electron microscope (SEM) to obtain high magnification images of Al granule surfaces; the instrument was fitted with an energy dispersive X-ray detector (EDX) for surface elemental analysis.

Particle size analysis: was determined in a Camsizer X2 (Retsch Technologies). For the measurements, ca. 1 g of particles were placed in the sample holder and the granules were dispersed in air flow through a Venturi nozzle (dispersion pressure was set at 95 kPa) before reaching the measurement field to avoid agglomerations. During measurement, the dispersed particle stream passes through two LED stroboscopic light waves, with the shadow projections of the particles being recorded by two digital cameras.

3. Results and discussion

3.1. Effect of temperature and NaOH molarity

In case of temperature, higher temperatures typically accelerate chemical reactions. To evaluate this effect in Al-water reactions, tests were performed by adding 400 mg of Al6060 cylindrical cut wire granules (⌀ = 1.0 mm, KrampeHarex) in a 3 M NaOH solution at temperatures between 50 and 80 °C. Fig. 1a shows the cumulative H_2 formation in moles as a function of time; the plots evidence faster conversions at higher temperatures. While about 17 min were needed to convert half of the Al at 50 °C, and only 5 min were required at 80 °C.

The reaction between Al and water is considered a first-order reaction dependent on the Al concentration as given in eq. (4).

$$r = k[Al]^n \quad \text{eq. 4}$$

where r is the reaction rate (mol·L^{-1}·s^{-1}), K is a reaction constant (s^{-1}), $[Al]$ is the Al concentration available for reaction (mol·L^{-1}) and n is the reaction order, in this case 1.

The first-order was verified by performing tests with varying amount of Al granules (from 100 to 500 mg), which led to a linear correlation between H_2 production rates and the Al concentration (Fig. S5a).

The relationship between temperature and the rate constant (K) is quantitatively described by the Arrhenius equation (eq. (5)), which states that K, and therefore the reaction rate, increases exponentially with temperature.

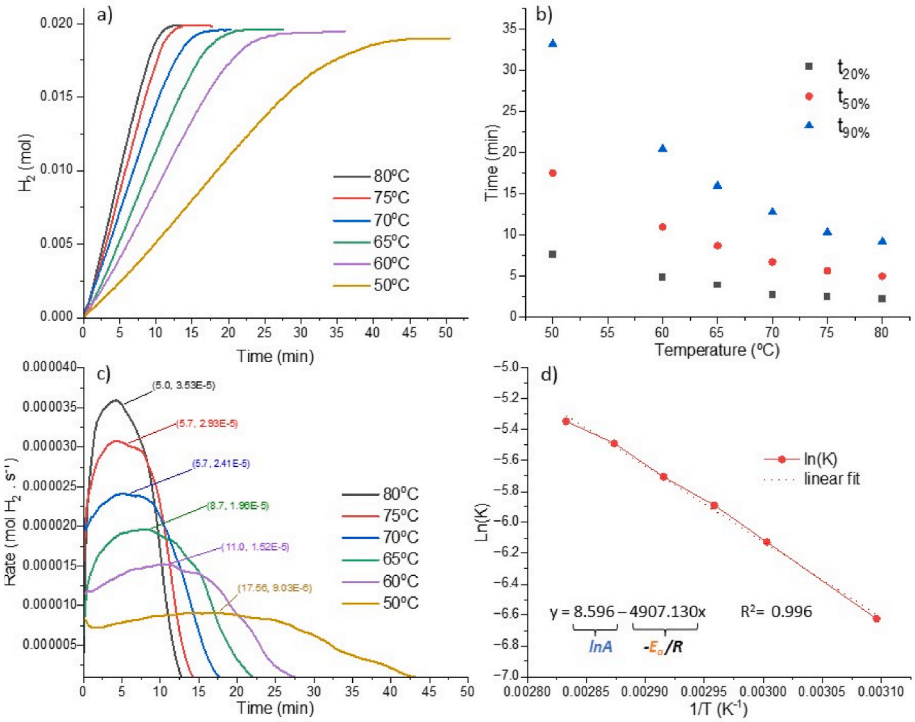


Fig. 1. Al-water reaction results at different temperatures using Al6060 cylindrical cut wire and 3 M NaOH solutions: a) H_2 evolution over time, b) comparison of $t_{20\%}$, $t_{50\%}$ and $t_{90\%}$, c) H_2 production rate over time illustrating the rate values at $t_{50\%}$ from which k is derived, and d) derivation of A and E_a values from the Arrhenius equation. Data in panel c was smoothed via 10-point adjacent averaging.

$$K = Ae^{-\frac{Ea}{RT}} \quad \text{eq. 5}$$

Where A is a pre-exponential factor related to the frequency of correctly oriented collisions between reactants (s^{-1}), e is the base of the natural logarithm (Euler's number, 2.71828), E_a is the activation energy ($J \bullet mol^{-1}$), R is the universal gas constant (8.3145 $J \bullet mol^{-1}\ K^{-1}$) and T is the absolute reaction temperature (K).

The exponential dependency of the Al-water reaction rate on temperature can be visualized in Fig. 1b where the reaction times obtained at 20%, 50% and 90% conversion – denoted as $t_{20\%}$, $t_{50\%}$ and $t_{90\%}$ respectively – are plotted as function of temperature. For this calculation, the total H_2 mol obtained after each test was considered as 100% conversion.

The rection rate in Fig. 1c corresponds to the derivative of Fig. 1a and is plotted as reaction rate in mol of H_2 per second as a function of time. Fig. 1c shows that for all temperatures the rates increase in the first half of reaction followed by a gradual rate decrease in the second half. The figure as well as Table 1 include the reaction rate values at $t_{50\%}$ which approximate the maximum rates obtained at each temperature.

In order to calculate the E_a of the reaction, K values for each temperature were derived dividing the reaction rate at $t_{50\%}$ conversion (Fig. 1c), by the Al concentration remaining at the same time (i.e. 0.15 $mol \bullet L^{-1}$). Plotting $\ln(K)$ vs $1/T$ a linear correlation is obtained where E_a and A can be derived from the slope and intercept, respectively (Fig. 1d). The $t_{20\%}$, $t_{50\%}$ and $t_{90\%}$ values as well as K, E_a, A and R^2 values derived in this analysis are given in Table 1. The E_a determined was 40.8 $kJ \bullet mol^{-1}$, which is within the range of values found in other studies (i.e. 24–80 $kJ \bullet mol^{-1}$) [67,73–75]. Note that the E_a reported here as well as the performance profiles may be somewhat different for other Al6060 sources. Variations are expected due to differences in composition and manufacturing process of granules from different suppliers.

Regarding alkalinity, increasing pH of solutions is known to accelerate the Al-water reaction due to a more efficient removal of the protective Al_2O_3 layer. This effect was investigated for Al6060 cylindrical granules at 60 °C using NaOH solutions of 1 M, 1.5 M, 2 M, 3 M and 6 M. As shown in Fig. 2a, the H_2 evolution trends obtained evidenced a significant increase of the reaction rate with NaOH molarity. The reaction time at 50% conversion for example was ca. 19 min in 1 M solution, while in 6 M solution it was only 10 min. Fig. 2b illustrates $t_{20\%}$, $t_{50\%}$ and $t_{90\%}$ as function of NaOH molarity (see tabulated data in Table 1), the profiles indicate that reaction rate also has an exponential response to the alkalinity or reaction media.

Determination reaction times provided here as function of temperature and alkalinity is of importance to define optimal conditions when using Al6060 cylindrical granules. The exponential profiles obtained in Figs. 1b and 2b imply that reaction rates improve sharply at milder range of conditions (from 1 to 2 M NaOH or from 50 to 70 °C) but rate improvement becomes gradual >2 M NaOH and >70 °C. Hence, the latter values are proposed as boundary conditions for Al-water reactions using Al6060 cut wire.

3.2. Effect of Al of mechanical and thermal treatments

3.2.1. Effect of mechanical treatment

Reaction kinetics between a solid and a fluid strongly depend on the surface area of the solid [76], which is inherently linked to its morphology and surface topology. In order to study the effect of granule morphology, Al6060 cylindrical cut wire granules (from Kumichel) were compared to rounded ones of equivalent size (⌀ = ca. 1.0 mm). The rounded Al granules were provided by the same supplier and are manufactured by subsequent mechanical treatment of the cut wire. This guarantees that same Al material is being compared in this study, allowing any differences in reaction kinetics to be attributed solely to granule morphology and mechanical treatment.

The SEM images of unreacted granules are given in Fig. 3 and the images show different surface topology for both types of granules. Cut wire cylinders exhibit a smooth curved surface (Fig. 3b), as well as a rough base (Fig. 3b). Rounded particles on the other hand display exclusively smooth but irregular morphology on the entirety of the spherical surface (Fig. 3d–e).

The Al-water reactions using different granule morphologies were performed in 2 M NaOH solutions at 65 °C (Fig. 4 and Table 2). These conditions were chosen as representative according to the work described in Section 3.1. The H_2 evolution plot in Fig. 4a indicates that the two granule morphologies exhibit different reaction kinetics; hence, the cylindrical granules react faster, resulting in $t_{50\%}$ values of 7.6 and 10.2 min for cylindrical and rounded granules, respectively (Table 2).

The reaction rates as a function of time give further information on Al-water reaction mechanism, and the different rate profiles in Fig. 4b suggest that both granule shapes respond to different mechanisms. The reaction rate using cylindrical granules gradually increases at the beginning of the reaction, it reaches a maximum of 0.0015 mol/min after 7 min and decreases then to 0 mol/min after 25 min. Such profile – exhibiting a defined maximum – is representative of reactions in porous solids where kinetics are described by the random pore model. In this mechanism the reaction occurs partially within the inner pore system of the solid [76,77]; as the reaction progress, the pores become deeper which results in a surface area increase enhancing reaction rates at early stages of the reaction [78].

In contrast to the cylinders, the rate profile for the rounded granules

Table 1
$t_{20\%}$, $t_{50\%}$ and $t_{90\%}$ values obtained during reaction oof Al6060 cylindrical cut wire (KrampeHarex) at various temperatures and NaOH molarities. The table also includes H_2 production rate and K values, as well as the E_a, A and R^2 derived from fitting the data to Arrhenius equation.

	Temperature (°C)	Molarity (M)	$t_{20\%}$ (min)	$t_{50\%}$ (min)	$t_{90\%}$ (min)	H_2 rate at $t_{50\%}$ ($mol \cdot s^{-1}$)	$K(s^{-1})$*
Temperature	50	3	7.64	17.56	33.23	9.03E-6	0.00122
	60		4.85	11.01	20.47	1.52E-5	0.00205
	65		3.92	8.72	16.00	1.96E-5	0.00265
	70		2.77	6.74	12.79	2.41E-5	0.00325
	75		2.50	5.66	10.37	2.93E-5	0.00396
	80		2.22	5.00	9.21	3.53E-5	0.00476
NaOH molarity	60	1	7.51	18.96	36.23	–	–
		1.5	6.47	15.21	28.56	–	–
		2	5.03	12.41	23.62	–	–
		3	4.85	11.01	20.47	–	–
		6	4.11	9.66	18.19	–	–
As received	65	2	4.27	10.34	19.86	–	–
Annealed	65	2	5.55	16.45	43.67	–	–
Arrhenius fit	E_a ($J \cdot mol^{-1}$)		40800.3				
	A (s^{-1})		7383.4				
	R^2		0.996				

* Derived from reaction rate at $t_{50\%}$.

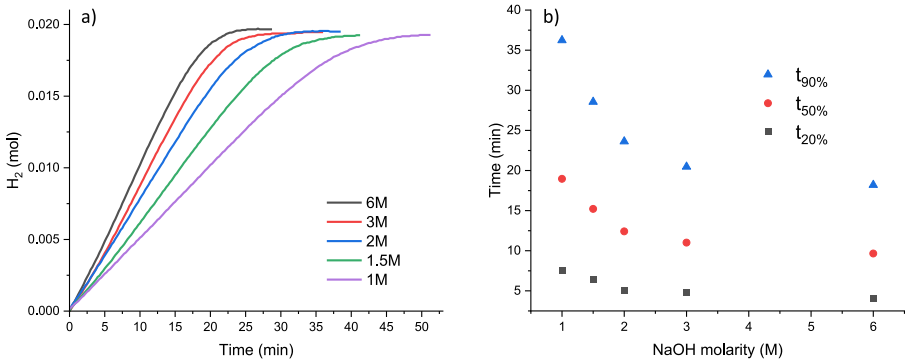


Fig. 2. Al-water reaction results using Al6060 cylindrical cut wire, and solutions with different NaOH molarities at 60 °C: a) H_2 evolution over time, b) comparison of $t_{20\%}$, $t_{50\%}$ and $t_{90\%}$.

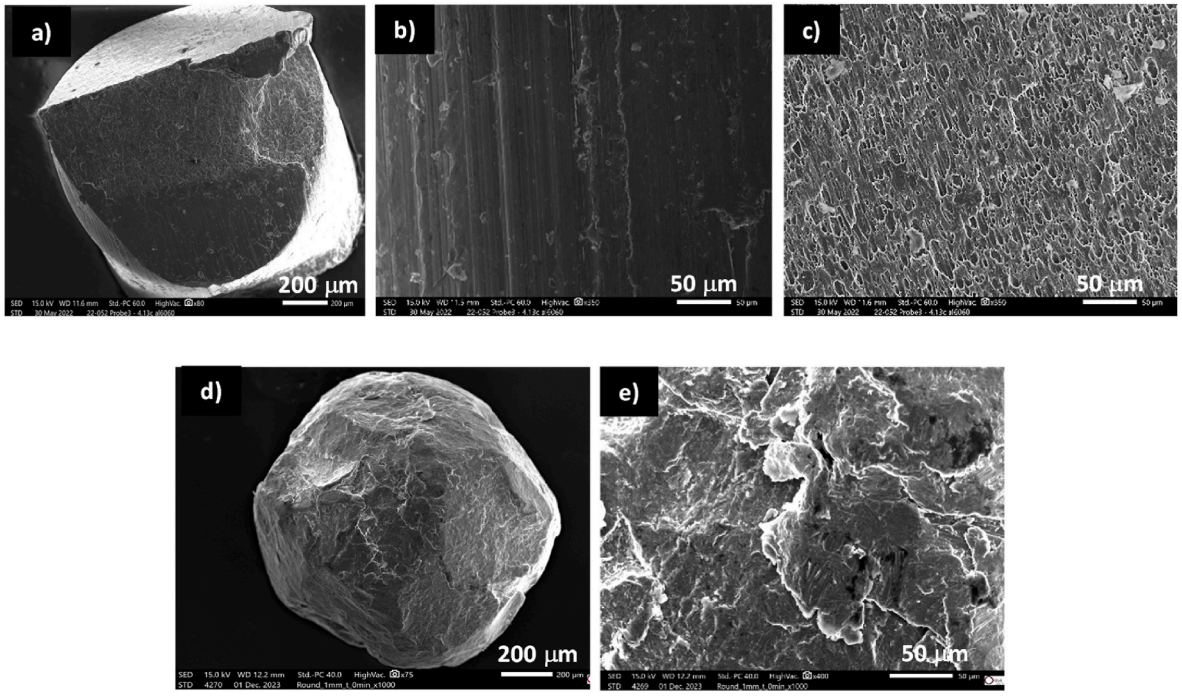


Fig. 3. SEM images of cylindrical and rounded Al6060 cut wire granules. a) Cylindrical granule, b) smooth curved surface in cylindrical granule, c) rough base of the cylindrical granule, d) rounded granule, e) irregular surface in the rounded granule.

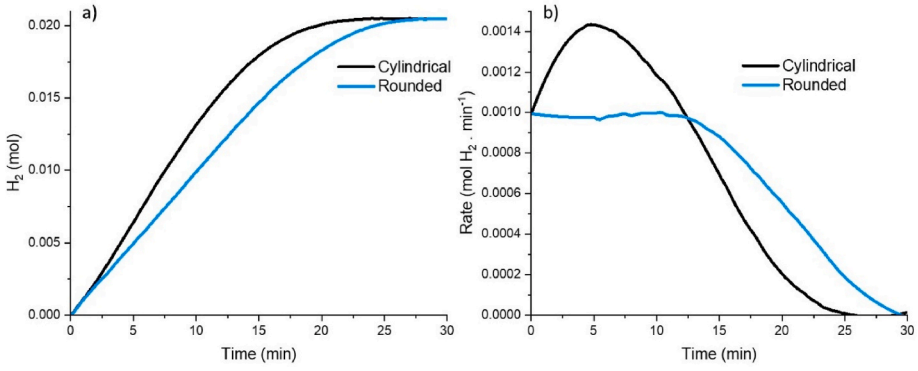


Fig. 4. Results for Al-water reaction for Al6060 cylindrical and rounded granules (ca. 1.0 mm) at 65 °C, 2 M NaOH; a) H_2 evolution as a function of time and b) reaction rate over time. Data in panel b was smoothed via 10-point adjacent averaging.

Table 2
$t_{20\%}$, $t_{50\%}$ and $t_{90\%}$ values obtained during reaction (65 °C and 2 M NaOH) of 400 mg of Al6060 cylindrical and rounded granules (Kuhmichel) of different sizes. The table also includes H_2 production rates measured at $t_{50\%}$.

	Diameter (mm)	$t_{20\%}$ (min)	$t_{50\%}$ (min)	$t_{90\%}$ (min)	H_2 rate at 50% conv. (mol·s^{-1})
Cylindrical	0.6	2.52	5.95	12.31	2.76E-05
	0.8	3.20	7.53	14.75	2.33E-05
	1.0	3.36	7.67	15.70	2.22E-05
	1.2	4.65	10.50	20.87	1.66E-05
Rounded	0.6	2.53	6.87	14.03	2.22E-05
	0.8	3.25	8.24	16.29	2.02E-05
	1.0	4.09	10.36	20.29	1.66E-05
	1.2	4.53	11.25	21.98	1.52E-05

exhibits a plateau at 0.0015 mol/min in the first half of the reaction; in the second half the rate gradually decreases reaching 0 mol/min after 30 min. Such profile – with no initial rate increase – suggests greater contribution of shrinking core reaction mechanism in rounded granules which is typical of non-porous materials. In this mechanism the reaction occurs at the outer surface, the diameter of the particle shrinks homogeneously as it gets consumed, and reaction rates decrease gradually over time leading to overall lower reaction rates than for porous materials.

SEM images of granules recovered after 50% conversion (2 M NaOH solution at 65 °C) give further insight into the rate profiles obtained. In the case of cylindrical granules (Fig. 5a), the base becomes highly porous at $t_{50\%}$ and exhibits pores of 2–25 μm (Fig. 5b and Fig. S6). This porosity goes in line with the random pore-like kinetics previously observed. Note that a secondary phase seems to accumulate in the walls of the pores (Fig. S6), SEM-EDX analyses in Fig. 5e–f indicate that such phase is composed of Mg and Si. These comprise the main alloying elements in Al6060 which likely precipitate in the form of oxides within the pores as the granules get consumed.

It must be highlighted here that the pores are present exclusively on the cylinder base, and that they appear aligned along the central axis of the cylindrical granules. This phenomenon can be tentatively ascribed to the Al6060 microstructure. The cut wire likely contains grain boundary phases that are oriented along the central axis as a result of extrusion during the wire manufacturing process. In Al6060, these boundaries are known to cause localized corrosion [71,79]. In this manuscript, we propose that the alignment of boundary phases in the cut wire sets the pathway for corrosive attack into directional pore formation during the Al-water reaction.

In case of the rounded granules – manufactured by mechanical treatment of cut wire cylinders – most of the surface remains smooth at

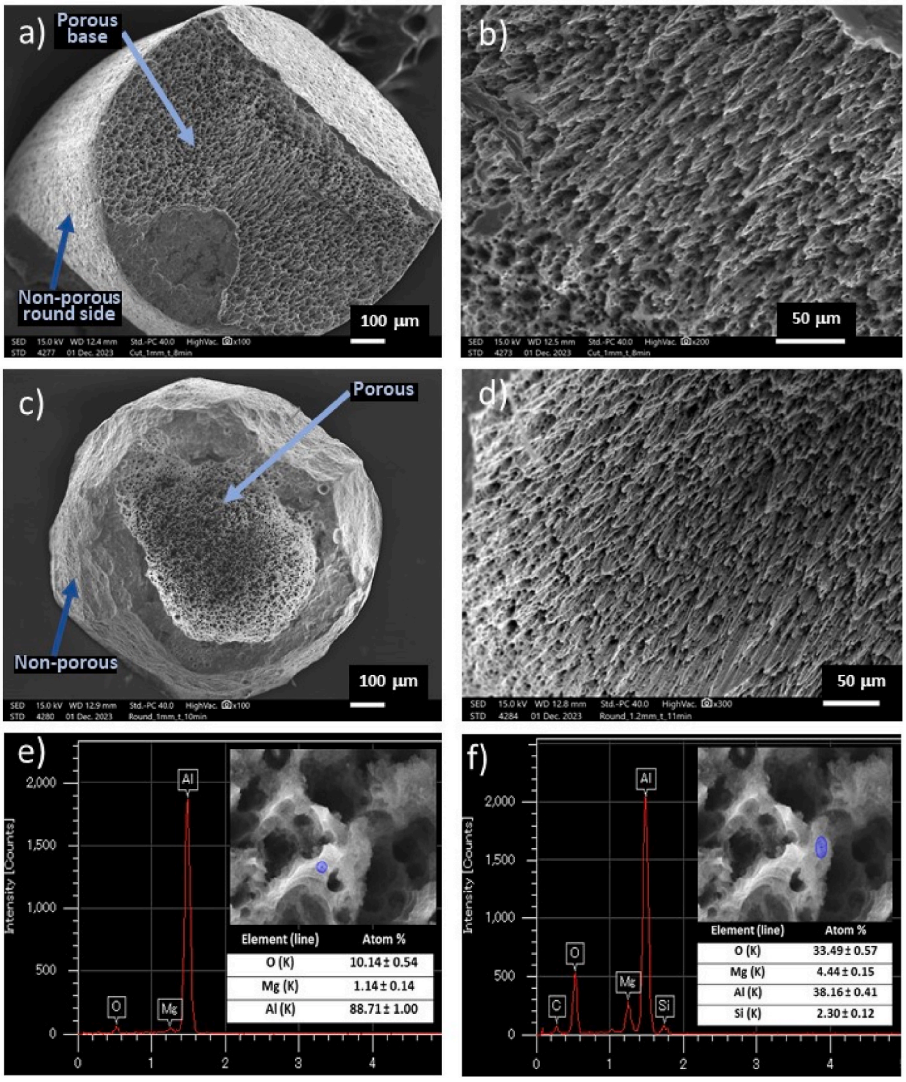


Fig. 5. SEM images of Al 6060 granules recovered after 50% conversion (Kuhmichel, 1.0 mm, 2 M NaOH - 65 °C): a-b) cylindrical, c-d) rounded and e-f) SEM-EDX analysis of the unreacted Al and the secondary phase observed in the interior of the pore.

$t_{50\%}$, but a clearly porous area is also observed (see arrows in Fig. 5c). The pores exhibit a defined directionality (Fig. 5d) similar to that of the cylindrical granules. This suggests that the mechanical treatment used for rounding modifies the Al microstructure in the granule outer shell while the inner core remains unmodified. Hence, once the outer shell is consumed during reaction, the unmodified inner microstructure gets exposed leading to directional pore formation.

In short, these findings suggest a rather complex granule depletion mechanism, where Al microstructure guides the granule reactivity. The coexistence of various surface morphologies during granule depletion (porous and non-porous) will lead to overlapping core-shell and porous reaction mechanism. A larger share of pore formation in cylindrical granules results in kinetic profiles dominated by the porous mechanism. In turn, partial modification of the microstructure in rounded granules leads to higher contribution of core-shell like kinetics and overall slower reaction rates.

3.2.2. *Effect of granule size on mechanical treatment*

Powders or small particles exhibit a high surface-to-bulk ratio and faster Al-water reaction than larger granules. In case of granules with cylinder and sphere geometries, the surface-to-bulk ratio decreases exponentially with increasing granule size (Fig. S9); as a result, exponential size dependency can also be projected for reaction rates. Nevertheless, for the samples studied in this work, the surface provided by the porous structure is expected to partially mitigate such size dependency.

For a close evaluation of size effects, Al6060 granules with custom-made diameters of ca. 0.6, 0.8, 1.0 and 1.2 mm were purchased for both, cylindrical and spherical morphologies. The granule size measurements (Fig. 6) reveal that the samples comprise a narrow and well resolved size distribution which ensures an accurate size-activity dependency evaluation.

The H_2 evolution from Al-water reactions (2 M NaOH and 65 °C) using different granule sizes is plotted in Fig. 7a–d while the $t_{20\%}$, $t_{50\%}$ and $t_{90\%}$ as function of granule size is given in Fig. 4e and Table 2. The general trends show shorter reaction times for the cylindrical granules than for rounded ones in line with its higher share of porous reaction mechanism observed in the previous section. As expected, the reactions are also faster when smaller granules are used, nevertheless the rate-size dependency is not exponential and the two granules used exhibit different dependencies.

For a more detailed discussion on these differences, we commence by drawing the attention to the $t_{90\%}$ values of 0.6 mm granules which correspond to 12.3 and 14.0 min for cylindrical and rounded granules, respectively. As expected, for larger Al grains, the reaction time increases. Up to 1.0 mm granules, the reaction time increase is more severe for the rounded ($t_{90\%}$ = 20.3 min) than for the cylindrical ($t_{90\%}$ = 15.7 min) granules; this can be attributed to the fact that the more porous nature of the cylindrical samples partially mitigates the loss of reactive surface area in larger granules. For the 1.2 mm granules however, the $t_{90\%}$ of both morphologies converged into similar values (20.9 and 22.0 min) and the reaction profiles look in fact comparable (Fig. 7d). Similar trends were also observed for $t_{20\%}$ and $t_{50\%}$.

The reaction rates in Fig. 8 and Table 2 give further insight into these trends. The rate profiles in the cylindrical samples (Fig. 8a) are in accordance with those of porous materials, and in all cases the profiles exhibit a reaction rate increase during the first 5–10 min of reaction followed by a rate decrease.

In contrast, for the rounded granules (Fig. 8b) the rate increase is less evident as they exhibit a profile closer to that of non-porous solids. If we look at the initial stages of reaction, the rates decrease steeply in 0.6 mm rounded sample (from ca. 0.0016 to 0.0013 mol/min after 10 min). The initial rate decrease is less marked in larger granules. For 1 mm granules for example, the reaction rate remains relatively constant (ca. 0.00010 mol/min) in the first 10 min. A rate increase can be even observed for 1.2 mm rounded granules (from 0.00085 to 0.00095 mol/min at 5–10 min) which points to an increased contribution of porous reaction mechanism for larger granules. Thus, the authors propose that while the granules exhibit an overlap of core-shell and porous mechanisms, the extent to which these mechanisms contribute is size dependent. For larger particles with lower surface-to-bulk ratio, the porous reaction mechanism driven by the granule core microstructure contributes more.

The presence of overlapping mechanisms is supported by digital microscopy images (Fig. 9) taken for 1 mm granules recovered at $t_{50\%}$ and $t_{90\%}$ (2 M NaOH solution 65 °C). In the case of the cylindrical granules, the cylinder base and the interior is seen to consume first via the faster random pore mechanism. This leads to a hole in the centre of the particle and only the outer shell is left at $t_{90\%}$, resulting in a ring-shaped particle (Fig. 9c-top). We propose that beyond this point the shrinking core mechanism dominates in the cylindrical granules.

In the case of rounded granules, a hole appears after $t_{50\%}$, resulting in a partially hollow particle. Representative image of a granule at $t_{90\%}$ shows how the inside has consumed preferentially, leading to a ring-shaped particle in a similar fashion as the cylindrical granule (Fig. 9c-down). Further microscopy images for 0.6–1.2 mm granules at $t_{50\%}$ showing the porous core can be found in Fig. S7 and Fig. S8. Note that

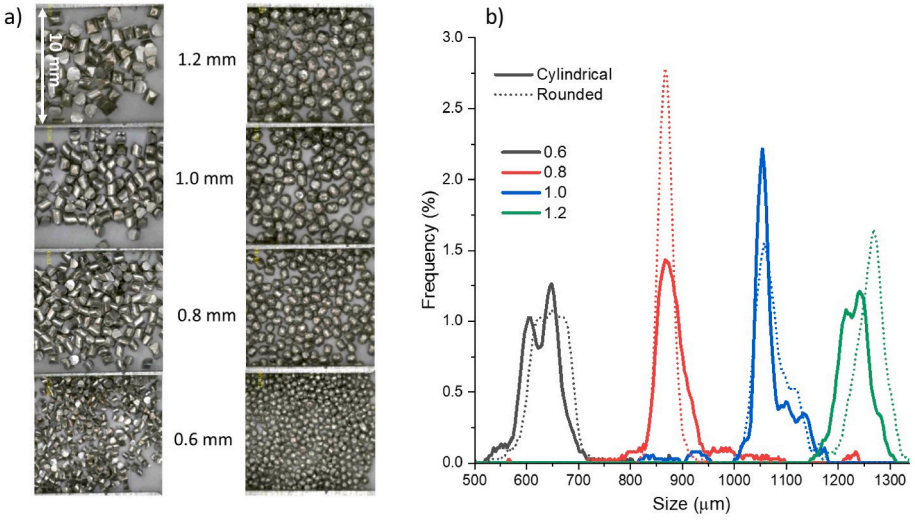


Fig. 6. Illustration of morphologies of Al6060 granules used for evaluation of shape and size dependency in Al-water reactions: a) digital microscopy images for cylindrical (left) and rounded (right) granules and b) grain size distributions measured.

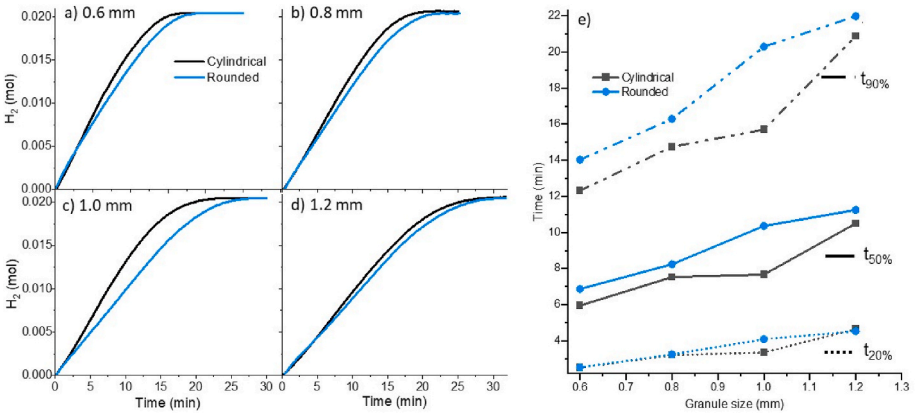


Fig. 7. Size dependency on Al-water reactions in 2 M NaOH solution at 65 °C for Al6060 cylindrical and rounded granules. Left: H_2 evolution for 0.6 mm (a), 0.8 mm (b), 1.0 mm (c) and 1.2 mm (d) granules. Right: $t_{20\%}$ $t_{50\%}$ and $t_{90\%}$ vs granule size (e).

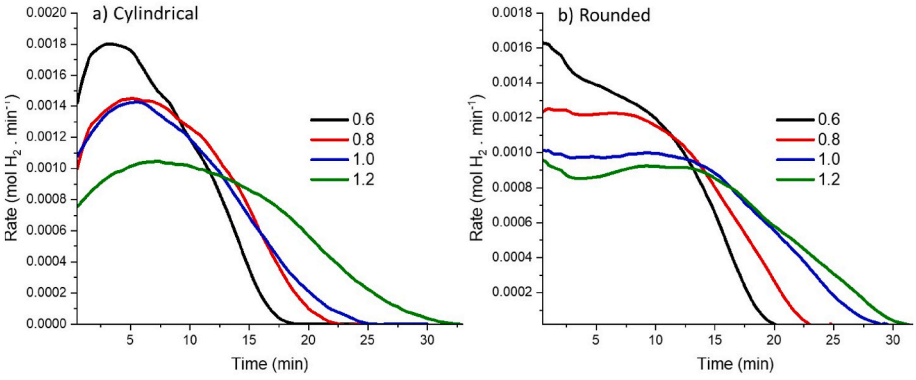


Fig. 8. Reaction rates obtained for Al6060 granules of different sizes at 65 °C and 2 M NaOH: a) cylindrical and b) rounded. The data was smoothed via 10-point adjacent averaging.

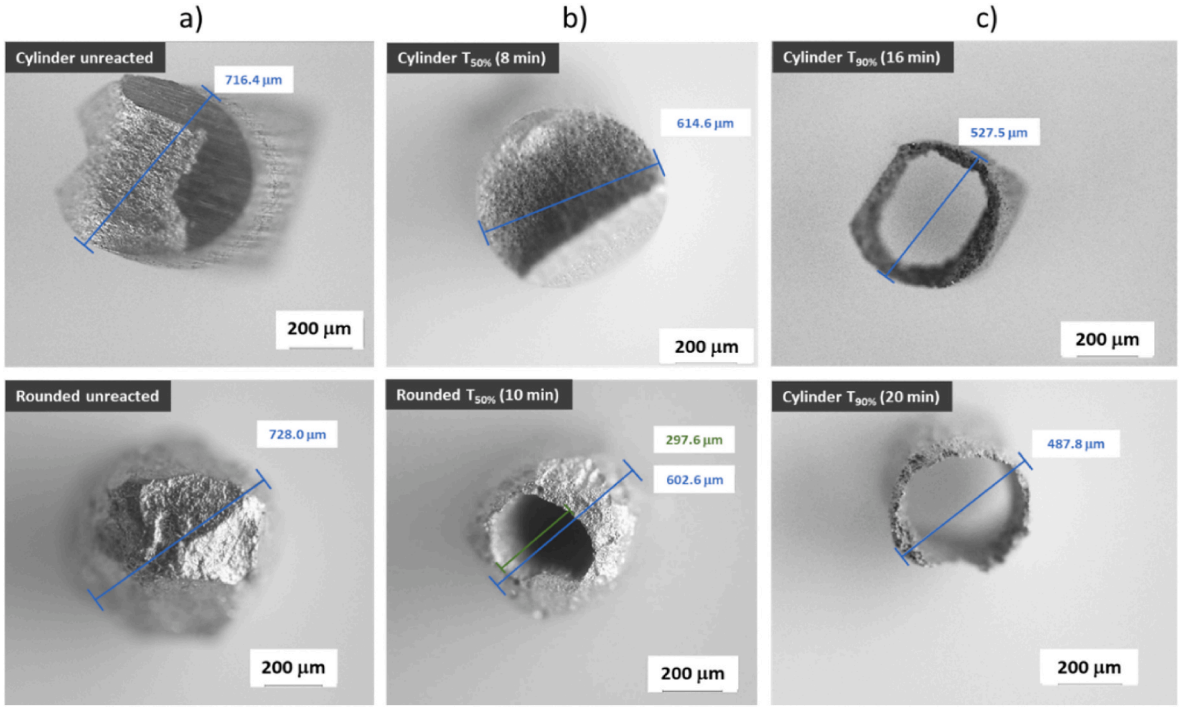


Fig. 9. Digital microscopy images of cylindrical (top) and rounded (bottom) Al6060 granules of 1.0 mm before and after reaction in 2 M NaOH at 65 °C: a) before reaction, b) after 50% conversion, and c) after 90% conversion.

the porous region responsible for hollow structure is comparatively smaller in the rounded granules. For 50% reacted granules in Figs. 5a and 9b top for example, the porous region in the cylinders appears to cover most of the granule cross section. In contrast, the rounded granules exhibit a smaller area relegated to the inner core (Figs. 5c and 9b bottom). A reduced porous region resulting from microstructure modification of outer shell during the mechanical treatment explains the overall slower reaction in the rounded granules. The contribution of porous and non-porous reaction mechanisms of these granules is size dependant as is affected by the surface to bulk ratio.

The authors propose that a mechanical treatment of cut wire cylinders for granule rounding alters the microstructure of the outer shell. This leads to a decreased contribution of random pore mechanisms as only the inner core of the granule maintains the microstructure responsible for pore formation. The porous mechanism in rounded granule will only takes place at later reaction stages once the outer shell is consumed and the inner core microstructure is exposed to the reaction media. At the final stages of reaction the pores are consumed and only the slow reacting shell remains which consume under shrinking-core mechanism. Fig. 10 shows a schematic representation of granule depletion processes proposed by the authors, which illustrates a possible sequence of dominant kinetic mechanisms during the Al-water reaction for cut wire granules.

3.2.3. *Effect of thermal treatment*

To gain further insights into the link between Al microstructure and reaction mechanism, cylindrical Al6060 granules (KrampeHarex) were subjected to solution annealing at 530 °C. Such procedure is known to alter the Al microstructure by decreasing defects in grain boundaries and dissolving intermetallics of alloying elements in the Al matrix. The as received and annealed granules were tested for Al-water reaction at 2 M NaOH and 65 °C.

Fig. 11a shows the cumulative H_2 evolution indicating that annealing renders Al granules with significantly slower kinetics. Hence, the $t_{20\%}$, $t_{50\%}$ and $t_{90\%}$ values (Table 1) comprise 4.3, 10.3 and 19.9 min respectively for the as received granules while for the annealed granules the values increase to 5.6, 16.5 and 43.7 min.

The rate profiles in Fig. 11b suggest that the two granules follow different kinetic mechanisms. In case of the as received granules, the rate increases in the first half of reaction as it is expected from reaction in porous solids; a reaction rate maxima of 0.0011 mol/min is obtained at 12 min. In contrast, the annealed granules show a rate profile typical for reactions in non-porous solids as the rates decrease continuously from an initial rate of 0.00075 mol/min to 0 mmol/min.

SEM images of samples recovered after 50% conversion (65 °C, 2 M NaOH) go in line with the reaction rate profiles obtained. The porous surface observable in the as received material (Fig. 12a–b) is absent in the annealed sample (Fig. 12c–d). This indicates that changes in Al6060 microstructure upon annealing prevents formation of porous surfaces under reactive conditions which corroborates the link between microstructure and reaction rates.

4. Conclusions

Past research on Al-water reactions focused mainly on the use of Al powder or expensive activation approaches to obtain fast reaction kinetics. Considering the ignition risk of metal powders, this work evaluates the use of Al6060 cut wire granules (>0.5 mm) as affordable and safe fuel. These granules are readily commercially available, they exceed the size for explosion risk and contain alloying elements (i.e. Mg, Si) which can potentially make them susceptible for corrosive attack favouring fast Al-water kinetics. To evaluate reaction parameters using such granules, several tests were performed by varying the temperature and alkalinity, while the use of different granule morphologies was also studied.

This work led to the determination of the activation energy for Al6060 cut wire cylindrical granules (i.e. $E_a = 40.8$ kJ/mol). The results also defined the exponential H_2 evolution profiles as a function of temperature and alkalinity. These profiles allowed to propose 70 °C and 2 M NaOH solutions as the boundary conditions because more severe conditions did not yield significant improvements in reaction rates.

Al-water reaction rate profiles for cylindrical cut wire Al6060 pointed to reaction kinetics resembling random pore mechanism. In agreement, SEM images of partially reacted granules revealed the formation of directional porosity upon reaction. The pore formation – which favours fast kinetics – was tentatively attributed to the existence of directional grain boundaries in the Al. These boundaries likely derive from a combination of the alloying elements present in Al6060 (e.g. Mg, Si) and the wire extrusion manufacturing process. Same Al6060 cut wires rounded by mechanical treatment exhibited higher contribution of shrinking core-like mechanism and overall slower kinetics. This was explained by partial changes in the Al microstructure during the mechanical treatment. It was concluded that shrinking core and porous mechanisms overlap in the studied granules, and that the granule manufacturing process as well as the granule size determines which mechanism predominates in the overall reaction rate. The microstructure - activity link was corroborated by the slower kinetics and no pore formation observed in thermally treated (annealed) granules.

The present study brings new insight into the use of commercially available Al granules for the Al-water reaction in aqueous media and defines suitable reaction conditions. Importantly, the work shows that the particular granule depletion mechanism – via pore formation – renders Al6060 cut wire granules, both safe and reactive material for its use as ReMeF. The findings highlight the importance of the granule size and manufacturing process in favouring microstructures for fast Al-water reaction mechanism. This sets the groundwork for further

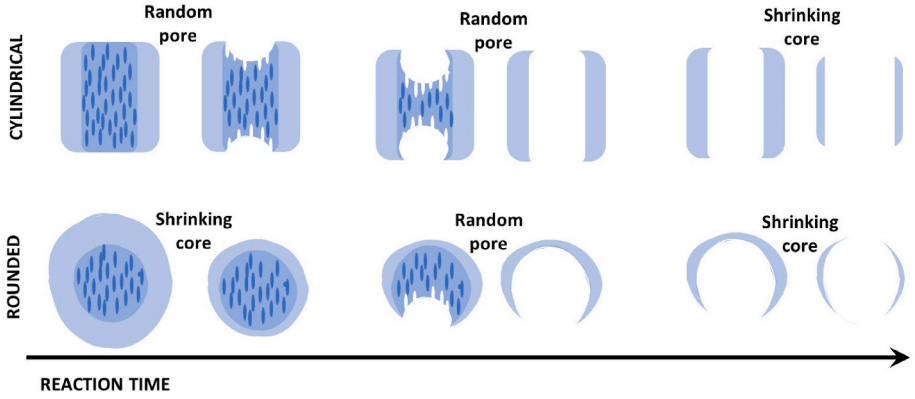


Fig. 10. Schematic representation of the dominating reaction models proposed at different stages of granule consumption for cylindrical and rounded Al6060 cur wires.

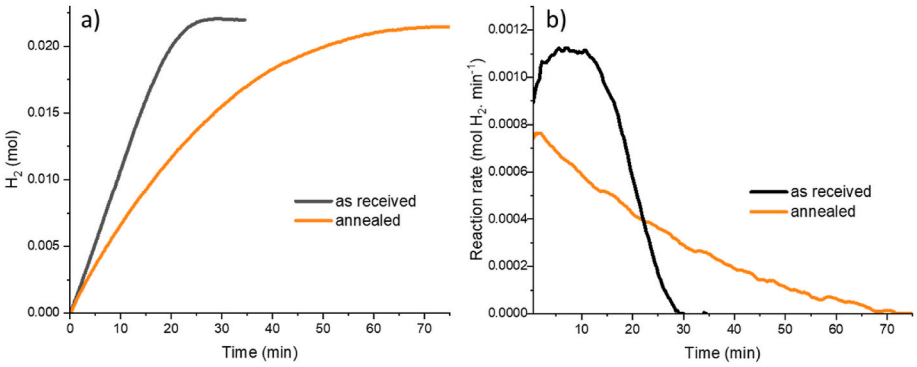


Fig. 11. Results for Al-water reaction (65 °C, 2 M NaOH) using Al6060 cylindrical granules (KrampeHarex, ca. 1.0 mm) before and after annealing: a) cumulative H_2 evolution over time and b) reaction rate over time. Data in panel b was smoothed via 14-point adjacent averaging.

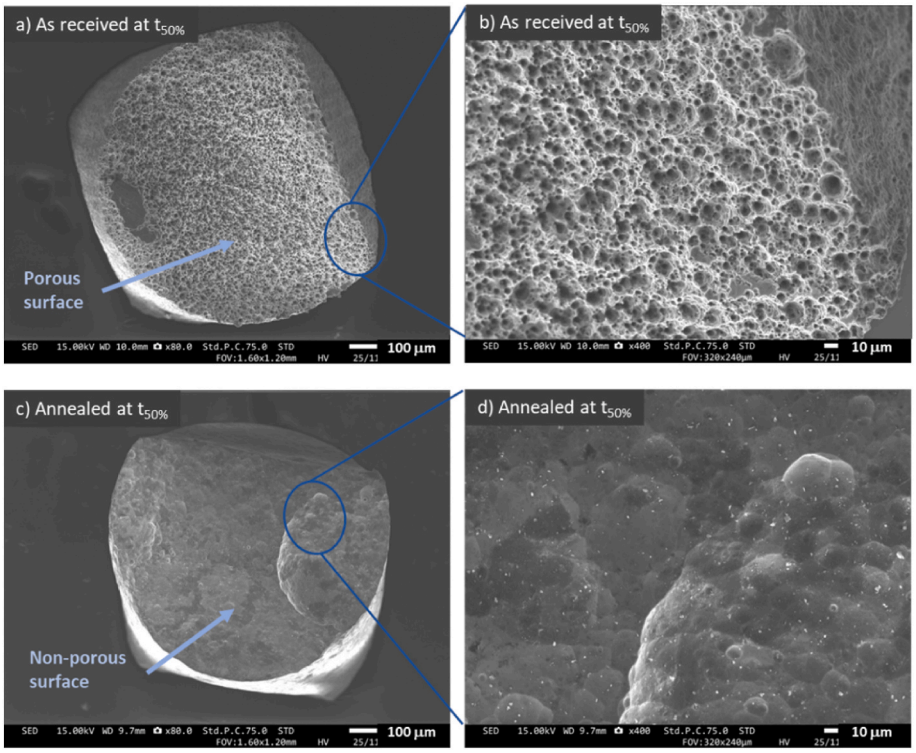


Fig. 12. SEM images of Al6060 cut wire cylindrical granules (KrampeHarex, ca. 1.0 mm) recovered after 50% conversion during Al-water reaction at 65 °C and 2 M NaOH: a-b) as received, and c-d) annealed at 530 °C for 20 min.

investigations into manufacturing techniques to design optimal Al granules for seasonal energy storage applications.

CRediT authorship contribution statement

M. Agote-Arán: Writing – original draft, Visualization, Supervision, Investigation, Conceptualization. **B. Welte:** Visualization, Supervision, Investigation, Data curation, Conceptualization. **R. Freeman:** Investigation, Data curation. **N. Mutti:** Investigation, Data curation. **M. Haller:** Writing – review & editing, Supervision, Investigation, Funding acquisition. **A. Heel:** Writing – review & editing, Supervision, Resources.

Declaration of competing interest

The authors declare that they have no known competing financial interests or personal relationships that could have appeared to influence the work reported in this paper.

Acknowledgement

The authors acknowledge financial support from the European Union's Horizon Europe research and innovation programme under Grant Agreement No. 101069492 and the Swiss State Secretariate for Education, Research and Innovation (SERI), contract number 22.00043. Views and opinions expressed are however those of the author(s) only and do not necessarily reflect those of the European Union. Neither the European Union nor the granting authority can be held responsible for them.

The authors thank Kuhmichel and KrampeHarex for providing Al6060 granules. Debra Cortés Gómez, Jan Allaart and Fabio Mazzoleni are thanked for their assistance during SEM and particle size distribution measurements. Jan Hüppi is acknowledged for the feedback on the initial draft. Erik Schmidt is kindly acknowledgement for performing Al annealing investigations (presented in section 3.2.3) as part of his semester work.

Appendix A. Supplementary data

Supplementary data to this article can be found online at https://doi.org/10.1016/j.ijhydene.2025.03.117.

References

[1] Bergthorson JM. Recyclable metal fuels for clean and compact zero-carbon power. Prog Energy Combust Sci 2018;68:169–96. https://doi.org/10.1016/j.pecs.2018.05.001.

[2] Trowell KA, Goroshin S, Frost DL, Bergthorson JM. Aluminum and its role as a recyclable, sustainable carrier of renewable energy. Appl Energy 2020;275:1–8. https://doi.org/10.1016/j.apenergy.2020.115112.

[3] Zhang J, Sun L, Sun T, Zhou H. Study on explosion risk of aluminum powder under different dispersions. J Loss Prev Process Ind 2020;64:1–8. https://doi.org/10.1016/j.jlp.2019.104042.

[4] Nie H, Zhang S, Schoenitz M, Dreizin EL. Reaction interface between aluminum and water. Int J Hydrogen Energy 2013;38:11222–32. https://doi.org/10.1016/j.ijhydene.2013.06.097.

[5] Haller MY, Carbonell D, Dudita M, Zenhäusern D, Häberle A. Seasonal energy storage in aluminium for 100 percent solar heat and electricity supply. Energy Convers Manag X 2020;5:100017. https://doi.org/10.1016/j.ecmx.2019.100017.

[6] Haller M, Amstad D, Dudita M, Carbonell D, Zenhäusern D. Hybrid seasonal storage of renewable heat and electricity with an Aluminium redox cycle. Rapperswil; 2021. https://doi.org/10.5281/zenodo.6327100.

[7] Haller MY, Amstad D, Dudita M, Englert A, Häberle A. Combined heat and power production based on renewable aluminium-water reaction. Renew Energy 2021;174:879–93. https://doi.org/10.1016/j.renene.2021.04.104.

[8] Haller M, Amstad D, Dudita M, Yvonne B. AlEnCycles Aluminium-Redox-Cycles for the production of heat and electricity for buildings based on renewable energies. Rapperswil; 2020. www.sorec.ch.

[9] Teichert M, Haller MY, Sick F. Aluminium redox cycle in comparison to pressurized hydrogen for the energy supply of multi-family houses. Appl. Energy Combust. Sci. 2023;13. https://doi.org/10.1016/j.jaecs.2022.100098.

[10] Gunnarsson G, Guðbjörg Ó, Sindri F, Magnússon JH. Aluminum electrolysis with multiple vertical non-consumable electrodes in a low temperature electrolyte. Light Met 2019:803–10.

[11] Singh K, Gunnarsson G, Magnusson JH, Haarberg GM, Saevarsdottir G. Performance evaluation of low-temperature KF-NaF-AlF 3 electrolytes for aluminum electrolysis using vertical inert Cu–Ni–Fe alloy anodes. J Electrochem Soc 2023;170:113507. https://doi.org/10.1149/1945-7111/ad0bae.

[12] Kaur P, Verma G. A critical assessment of aluminum-water reaction for on-site hydrogen-powered applications. Mater Today Energy 2024;40:1–29. https://doi.org/10.1016/j.mtener.2024.101508.

[13] Su M, Hu H, Gan J, Ye W, Zhang W, Wang H. Thermodynamics, kinetics and reaction mechanism of hydrogen production from a novel Al alloy/NaCl/C3N4 composite by low temperature hydrolysis. Energy 2021;218:1–12. https://doi.org/10.1016/j.energy.2020.119489.

[14] Petrovic J, Thomas G. Reaction of aluminum with water to produce hydrogen. U.S. Department of Energy; 2008. p. 1–26.

[15] Ouyang L, Liu M, Chen K, Liu J, Wang H, Zhu M, Yartys V. Recent progress on hydrogen generation from the hydrolysis of light metals and hydrides. J Alloys Compd 2022;910:1–22. https://doi.org/10.1016/j.jallcom.2022.164831.

[16] Bolt A, Dincer I, Agelin-Chaab M. A review of unique aluminum-water based hydrogen production options. Energy Fuels 2021;35:1024–40. https://doi.org/10.1021/acs.energyfuels.0c03674.

[17] Wang HZ, Leung DYC, Leung MKH, Ni M. A review on hydrogen production using aluminum and aluminum alloys. Renew Sustain Energy Rev 2009;13:845–53. https://doi.org/10.1016/j.rser.2008.02.009.

[18] Escobar-Alarcón L, Iturbe-García JL, González-Zavala F, Solis-Casados DA, Pérez-Hernández R, Haro-Poniatowski E. Hydrogen production by ultrasound assisted liquid laser ablation of Al, Mg and Al-Mg alloys in water. Appl Surf Sci 2019;478:189–96. https://doi.org/10.1016/j.apsusc.2019.01.213.

[19] Xu S, Zhao X, Liu J. Liquid metal activated aluminum-water reaction for direct hydrogen generation at room temperature. Renew Sustain Energy Rev 2018;92:17–37. https://doi.org/10.1016/j.rser.2018.04.052.

[20] Gai WZ, Tian S, Liu MH, Zhang X, Deng ZY. Synergistic effect and mechanisms of ultrasound and AlOOH suspension on Al hydrolysis for hydrogen production. Ultrason Sonochem 2022;90:1–8. https://doi.org/10.1016/j.ultsonch.2022.106189.

[21] Kumar D, Muthukumar K. An overview on activation of aluminium-water reaction for enhanced hydrogen production. J Alloys Compd 2020;835:1–10. https://doi.org/10.1016/j.jallcom.2020.155189.

[22] Dupiano P, Stamatis D, Dreizin EL. Hydrogen production by reacting water with mechanically milled composite aluminum-metal oxide powders. Int J Hydrogen Energy 2011;36:4781–91. https://doi.org/10.1016/j.ijhydene.2011.01.062.

[23] Liu Y, chao An J, zhong Jin W, Cui J, Zhang W. Insight into the effect of in addition on hydrogen generation behavior and hydrolysis mechanism of Al-based ternary alloys in distilled water—a new active Al-Ga-In hydrolysis hydrogen generation alloy. Int J Energy Res 2019;43:8973–84. https://doi.org/10.1002/er.4857.

[24] Yuan B, Tan S, Liu J. Dynamic hydrogen generation phenomenon of aluminum fed liquid phase Ga-In alloy inside NaOH electrolyte. Int J Hydrogen Energy 2016;41:1453–9. https://doi.org/10.1016/j.ijhydene.2015.10.044.

[25] Zhang X, Fang J, Feng Y, Zhang J, Guo R, Chen J. The mechanism of water decomposition on surface of aluminum and gallium alloy during the hydrogen production process: a DFT study. Int J Hydrogen Energy 2024;66:354–61. https://doi.org/10.1016/j.ijhydene.2024.04.107.

[26] Jang S, Jeghan SMN, Seon E, Tak Y, Kim M, Lee G. Unraveling the corrosion kinetics of gallium-aluminum for efficient hydrogen production from water at zero CO2 emission. Int J Hydrogen Energy 2023;48:13390–403. https://doi.org/10.1016/j.ijhydene.2022.12.185.

[27] Kandasamy J, Mutlu RN, Eroğlu E, Karaca M, Toffoli H, Gökalp İ. Hydrogen production using aluminum-water splitting: a combined experimental and theoretical approach. Int J Hydrogen Energy 2024;52:202–11. https://doi.org/10.1016/j.ijhydene.2023.04.068.

[28] Guo J, Su Z, Tian J, Deng J, Fu T, Liu Y. Enhanced hydrogen generation from Al-water reaction mediated by metal salts. Int J Hydrogen Energy 2021;46:3453–63. https://doi.org/10.1016/j.ijhydene.2020.10.220.

[29] Gai WZ, Zhang X, Yang Y, Deng ZY. Effect of crystalline phases of aluminum hydroxide catalysts on Al-water reaction. Int J Energy Res 2020;44:4969–76. https://doi.org/10.1002/er.5238.

[30] Fan MQ, Xu F, Sun LX. Studies on hydrogen generation characteristics of hydrolysis of the ball milling Al-based materials in pure water. Int J Hydrogen Energy 2007;32:2809–15. https://doi.org/10.1016/j.ijhydene.2006.12.020.

[31] Liu Y, Wang X, Liu H, Dong Z, Li S, Ge H, Yan M. Study on hydrogen generation from the hydrolysis of a ball milled aluminum/calcium hydride composite. RSC Adv 2015;5:60460–6. https://doi.org/10.1039/c5ra09200k.

[32] Ho CY, Huang CH. Enhancement of hydrogen generation using waste aluminum cans hydrolysis in low alkaline de-ionized water. Int J Hydrogen Energy 2016;41:3741–7. https://doi.org/10.1016/j.ijhydene.2015.11.083.

[33] Razavi-Tousi SS, Szpunar JA. Role of ball milling of aluminum powders in promotion of aluminum-water reaction to generate hydrogen. Metall Mater Trans 2014;1:247–56. https://doi.org/10.1007/s40553-014-0024-7.

[34] Razavi-Tousi SS, Szpunar JA. Effect of structural evolution of aluminum powder during ball milling on hydrogen generation in aluminum-water reaction. Int J Hydrogen Energy 2013;38:795–806. https://doi.org/10.1016/j.ijhydene.2012.10.106.

[35] Xiao F, Guo Y, Li J, Yang R. Hydrogen generation from hydrolysis of activated aluminum composites in tap water. Energy 2018;157:608–14. https://doi.org/10.1016/j.energy.2018.05.201.

[36] du Preez SP, Bessarabov DG. Hydrogen generation by the hydrolysis of mechanochemically activated aluminum-tin-indium composites in pure water. Int J Hydrogen Energy 2018:21398–413. https://doi.org/10.1016/j.ijhydene.2018.09.133.

[37] Wang H, Lu J, Dong SJ, Chang Y, Fu YG, Luo P. Preparation and hydrolysis of aluminum based composites for hydrogen production in pure water. Mater Trans 2014;55:892–8. https://doi.org/10.2320/matertrans.M2013425.

[38] He T, Wang W, Chen W, Chen D, Yang K. Reactivity of Al-rich Alloys with water promoted by liquid Al grain boundary phases. J Mater Sci Technol 2017;33:397–403. https://doi.org/10.1016/j.jmst.2016.11.013.

[39] An Q, Hu H, Li N, Liu D, Xu S, Liu Z, Wei C, Luo F, Xia M, Gao Q. Effects of Bi composition on microstructure and Al-water reactivity of Al-rich alloys with low-In. Int J Hydrogen Energy 2018;43:10887–95. https://doi.org/10.1016/j.ijhydene.2018.05.009.

[40] Yang B, Zhu J, Jiang T, Gou Y, Hou X, Pan B. Effect of heat treatment on Al–Mg–Ga–In–Sn alloy for hydrogen generation through hydrolysis reaction. Int J Hydrogen Energy 2017;42:24393–403. https://doi.org/10.1016/j.ijhydene.2017.07.091.

[41] He T, Xiong Y, Du S, Yuan Z, Liang X, Huttula M, Cao W. Impact of Li addition in Al-rich alloys on hydrogen production in water. J Mater Eng Perform 2019;28:2459–64. https://doi.org/10.1007/s11665-019-04019-w.

[42] Wei C, Liu D, Xu S, Cui T, An Q, Liu Z, Gao Q. Effects of Cu additives on the hydrogen generation performance of Al-rich alloys. J Alloys Compd 2018;738:105–10. https://doi.org/10.1016/j.jallcom.2017.12.152.

[43] Zhuk AZ, Shkolnikov EI, Borodina TI, Valiano GE, Dolzhenko AV, Kiseleva EA, Kochanova SA, Filippov ED, Semenova VA. Aluminium – water hydrogen generator for domestic and mobile application. Appl Energy 2023;334. https://doi.org/10.1016/j.apenergy.2023.120693.

[44] Davies J, Du Preez SP, Bessarabov DG. The hydrolysis of ball-milled aluminum–bismuth–nickel composites for on-demand hydrogen generation. Energies 2022;15. https://doi.org/10.3390/en15072356.

[45] Xiao F, Yang R, Gao W, Hu J, Li J. Effect of carbon materials and bismuth particle size on hydrogen generation using aluminum-based composites. J Alloys Compd 2020;817. https://doi.org/10.1016/j.jallcom.2019.152800.

[46] Rafi M, Kolupula AP, Vadali V S S S, Varam S. An overview of hydrogen generation by hydrolysis of Al and its alloys with the addition of carbon-based materials. Int J Hydrogen Energy 2023;48:21345–59. https://doi.org/10.1016/j.ijhydene.2022.12.318.

[47] Xiao F, Liang T, Liu Z, Yang R, Li J. Study on the effect of carbon materials with different morphologies on the hydrogen generation performance of aluminum: a strategy to control the hydrogen generation rate of aluminum. J Alloys Compd 2021;879. https://doi.org/10.1016/j.jallcom.2021.160376.

[48] Liao L, Guo X, Xu F, Sun L, Wang T, Zhou T, Li Y, Li J, Zhang K, Li B, Peng H, Zou Y, Zhang H. A high activity Al–Bi@C for hydrogen generation from Al-water reaction. Ceram Int 2021;47:29064–71. https://doi.org/10.1016/j.ceramint.2021.07.067.

[49] Su M, Hu H, Gan J, Ye W, Zhang W, Wang H. Thermodynamics, kinetics and reaction mechanism of hydrogen production from a novel Al alloy/NaCl/g-C3N4 composite by low temperature hydrolysis. Energy 2021;218. https://doi.org/10.1016/j.energy.2020.119489.

[50] Huang H, Shu D. A novel AlGa@Gr material for ultrasound enhanced hydrogen generation. Int J Hydrogen Energy 2021;46:39499–508. https://doi.org/10.1016/j.ijhydene.2021.09.143.
[51] Prabu S, Wang HW. Enhanced hydrogen generation from graphite-mixed aluminum hydroxides catalyzed Al/water reaction. Int J Hydrogen Energy 2020;45:33419–29. https://doi.org/10.1016/j.ijhydene.2020.09.036.
[52] Yi G, Derrick AT, Zhu Y, Free ML. A collector plate mechanism-based classical intergranular precipitation model for Al alloys sensitized at different temperatures. Metall Mater Trans A Phys Metall Mater Sci 2015;46:5393–406. https://doi.org/10.1007/s11661-015-3110-2.
[53] Searles JL, Gouma PI, Buchheit RG. Stress corrosion cracking of sensitized AA5083. Metall Mater Trans 2000;32A:2859–67.
[54] Nickel D, Dietrich D, Mehner T, Frint P, Spieler D, Lampke T. Effect of strain localization on pitting corrosion of an AlMgSi0.5 alloy. Metals 2015;5:172–91. https://doi.org/10.3390/met5010172.
[55] Brosi JK, Seifi SM, Lewandowski JJ. Delamination of sensitized Al-Mg alloy during fatigue crack growth in room temperature air. Metall Mater Trans A Phys Metall Mater Sci 2012;43:3952–6. https://doi.org/10.1007/s11661-012-1361-8.
[56] Meroueh L, Neil L, Eagar TW, Hart DP. Leveraging grain size effects on hydrogen generated via doped aluminum-water reactions enabled by a liquid metal. ACS Appl Energy Mater 2021;4:275–85. https://doi.org/10.1021/acsaem.0c02175.
[57] Kudryashova OB, Morozova ON, Antonnikova AA. Critical conditions of Al powder-water reaction in a heated stirred reactor. Int J Hydrogen Energy 2020;45:30957–65. https://doi.org/10.1016/j.ijhydene.2020.08.068.
[58] Rosenband V, Gany A. Application of activated aluminum powder for generation of hydrogen from water. Int J Hydrogen Energy 2010;35:10898–904. https://doi.org/10.1016/j.ijhydene.2010.07.019.
[59] Czech E, Troczynski T. Hydrogen generation through massive corrosion of deformed aluminum in water. Int J Hydrogen Energy 2010;35:1029–37. https://doi.org/10.1016/j.ijhydene.2009.11.085.
[60] Mahmoodi K, Alinejad B. Enhancement of hydrogen generation rate in reaction of aluminum with water. Int J Hydrogen Energy 2010;35:5227–32. https://doi.org/10.1016/j.ijhydene.2010.03.016.
[61] Yavor Y, Goroshin S, Bergthorson JM, Frost DL, Stowe R, Ringuette S. Enhanced hydrogen generation from aluminum-water reactions. Int J Hydrogen Energy 2013;38:14992–5002. https://doi.org/10.1016/j.ijhydene.2013.09.070.
[62] Gai WZ, Liu WH, Deng ZY, Zhou JG. Reaction of Al powder with water for hydrogen generation under ambient condition. Int J Hydrogen Energy 2012;37:13132–40. https://doi.org/10.1016/j.ijhydene.2012.04.025.
[63] Bolt A, Dincer I, Agelin-Chaab M. Experimental study of hydrogen production process with aluminum and water. Int J Hydrogen Energy 2020;45:14232–44. https://doi.org/10.1016/j.ijhydene.2020.03.160.
[64] Corsi JS, Fu J, Wang Z, Lee T, Ng AK, Detsi E. Hierarchical bulk nanoporous aluminum for on-site generation of hydrogen by hydrolysis in pure water and combustion of solid fuels. ACS Sustainable Chem Eng 2019;7:11194–204. https://doi.org/10.1021/acssuschemeng.9b00481.
[65] Lee T, Corsi JS, Wang L, Detsi E. Air-stable nanoporous aluminum/lithium borohydride fuel pellets for onboard hydrogen generation by hydrolysis with pure water. ACS Appl Energy Mater 2021;4:9742–50. https://doi.org/10.1021/acsaem.1c01825.
[66] Urbonavicius M, Varnagiris S, Mezulis A, Lesnicenoks P, Knoks A, Richter C, Milcius D, Meirbekova R, Gunnarsson G, Kleperis J. Hydrogen from industrial aluminium scraps: hydrolysis under various conditions, modelling of pH behaviour and analysis of reaction by-product. Int J Hydrogen Energy 2024;50:431–46. https://doi.org/10.1016/j.ijhydene.2023.09.065.
[67] Mezulis A, Richter C, Lesnicenoks P, Knoks A, Varnagiris S, Urbonavicius M, Milcius D, Kleperis J. Studies on water–aluminum scrap reaction kinetics in two steps and the efficiency of green hydrogen production. Energies 2023;16:5554. https://doi.org/10.3390/en16145554.
[68] Průša F, Vojtěch D, Michalcová A, Marek I. Mechanical properties and thermal stability of Al-Fe-Ni alloys prepared by centrifugal atomisation and hot extrusion. Mater Sci Eng, A 2014;603:141–9. https://doi.org/10.1016/j.msea.2014.02.081.
[69] Wang L, Makhlouf M, Apelian D. Aluminium die casting alloys: alloy composition. microstructure, and properties-performance relationships. 1995.
[70] Huttunen-Saarivirta E. Microstructure, fabrication and properties of quasicrystalline Al-Cu-Fe alloys: a review. J Alloys Compd 2004;363:154–78. https://doi.org/10.1016/S0925-8388(03)00445-6.
[71] Aristeidakis JS, Haidemenopoulos GN, Bjørge R, Marioara CD, Kamoutsi H, Giarmas E, Rafailidis N. Microstructural evolution in a 6060 extrudable Al-alloy: integrated modeling and experimental validation. Materials 2024;17. https://doi.org/10.3390/ma17030545.
[72] Beltiskus D. Reaction of aluminum with sodium hydroxide solution as a source of hydrogen. Electrochem. Soc. 1970;117:1097–9.
[73] Aleksandrov YA, Tsyganova EI, Pisarev AL. Reaction of aluminum with dilute aqueous NaOH solutions. Russ J Gen Chem 2003;73:729–34.
[74] Alviani VN, Setiani P, Uno M, Oba M, Hirano N, Watanabe N, Tsuchiya N, Saishu H. Mechanisms and possible applications of the Al–H2O reaction under extreme pH and low hydrothermal temperatures. Int J Hydrogen Energy 2019;44:29903–21. https://doi.org/10.1016/j.ijhydene.2019.09.152.
[75] El-Awady AA, Abd-El-Nabey BA, Aziz SG. Thermodynamic and kinetic factors in chloride ion pitting of aluminium metal corrosion, vol. 89; 1993. p. 795–802. https://doi.org/10.1039/FT9938900795.
[76] Dong L, Mazzarino I, Alexiadis A. Development of solid–fluid reaction models—a literature review. ChemEngineering 2021;5:3–31. https://doi.org/10.3390/chemengineering5030036.
[77] Bhatia SK, O Perlmutter D. A random pore model for fluid-solid reactions. AIChE J 1980;26:379–86. https://doi.org/10.1002/aic.690260308.
[78] Grasa G, Murillo R, Alonso M, Abanades JC. Application of the random pore model to the carbonation cyclic reaction. AIChE J 2009;55:1246–55. https://doi.org/10.1002/aic.11746.
[79] Sarafoglou PI, Serafeim A, Fanikos IA, Aristeidakis JS, Haidemenopoulos GN. Modeling of microsegregation and homogenization of 6xxx Al-alloys including precipitation and strengthening during homogenization cooling. Materials 2019;12:1–25. https://doi.org/10.3390/ma12091421.